# JCI The Journal of Clinical Investigation

# The hematopoietic stem cell MYB enhancer is essential and recurrently amplified during T-cell leukemogenesis

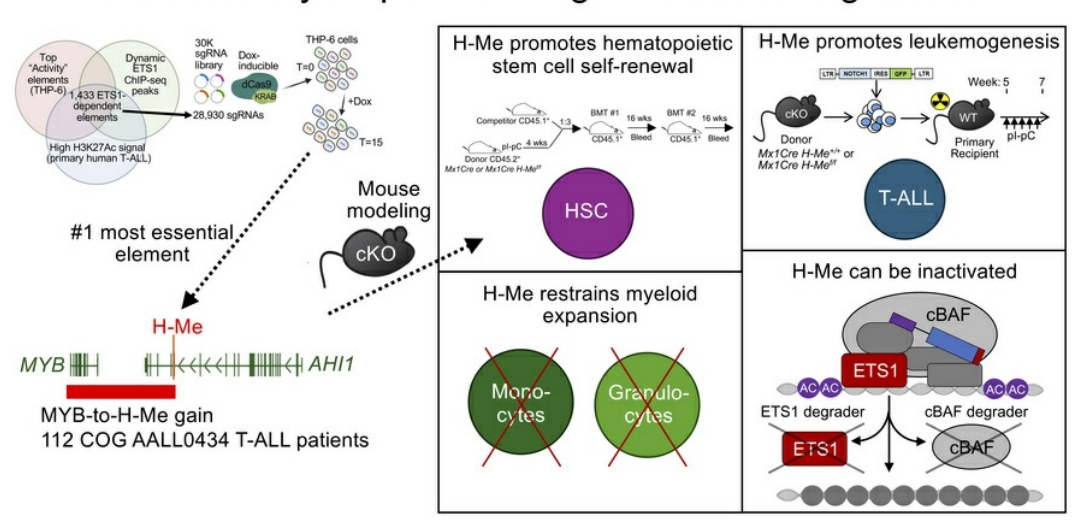
Carea Mullin, ..., Russell J.H. Ryan, Mark Y. Chiang

J Clin Invest. 2025. https://doi.org/10.1172/JCI187998.

Research In-Press Preview Cell biology Hematology Oncology

#### **Graphical abstract**

The hematopoietic stem cell MYB enhancer (H-Me) is essential and recurrently amplified during T-cell leukemogenesis



#### Find the latest version:



#### Title

The hematopoietic stem cell MYB enhancer is essential and recurrently amplified during T-cell leukemogenesis

#### **Authors**

Carea Mullin<sup>1,\*</sup>, Karena Lin<sup>2,\*</sup>, Elizabeth Choe<sup>1</sup>, Cher Sha<sup>3</sup>, Zeel Shukla<sup>1</sup>, Koral Campbell<sup>4</sup>, Anna C. McCarter<sup>5</sup>, Annie Wang<sup>1</sup>, Jannaldo Nieves-Salva<sup>6</sup>, Sarah Khan<sup>1</sup>, Theresa M. Keeley<sup>7</sup>, Shannon Liang<sup>1</sup>, Qing Wang<sup>1</sup>, Ashley F. Melnick<sup>2</sup>, Pearl Evans<sup>1</sup>, Alexander C. Monovich<sup>3</sup>, Ashwin Iyer<sup>8</sup>, Rohan Kodgule<sup>9</sup>, Yamei Deng<sup>10</sup>, Felipe da Veiga Leprevost<sup>10</sup>, Kelly R. Barnett<sup>11</sup>, Petri Pölönen<sup>12</sup>, Rami Khoriaty<sup>1</sup>, Daniel Savic<sup>11</sup>, David T. Teachey<sup>13</sup>, Charles G. Mullighan<sup>12</sup>, Marcin Cieslik<sup>10,14</sup>, Alexey I. Nesvizhskii<sup>10,14</sup>, Linda C. Samuelson<sup>7</sup>, Morgan Jones<sup>1</sup>, Qing Li<sup>1</sup>, Russell J. H. Ryan<sup>10,15</sup>, Mark Y. Chiang<sup>1,15</sup>

#### **Affiliations**

<sup>1</sup>Division of Hematology-Oncology, Department of Internal Medicine, University of Michigan School of Medicine, Ann Arbor, MI, USA; <sup>2</sup>Cellular and Molecular Biology Program, University of Michigan School of Medicine, Ann Arbor, MI, USA; <sup>3</sup>Immunology and Microbiology Program, Baylor College of Medicine, Houston, TX, USA <sup>4</sup>Molecular and Cellular Pathology Program, University of Michigan, Ann Arbor, MI, USA;; <sup>5</sup>Department of Anesthesiology, Perioperative and Pain Medicine, Stanford University, Stanford, CA, USA; <sup>6</sup>Immunology Program, University of Michigan School of Medicine, Ann Arbor, MI, USA; <sup>7</sup>Department of Molecular and Integrative Physiology, University of Michigan, Ann Arbor, MI; <sup>8</sup>Regeneron Pharmaceuticals, Tarrytown, NY, USA; <sup>9</sup>Department of Pathology and Immunology, WashU Medicine, St. Louis, MO; <sup>10</sup>Department of Pathology, University of Michigan, Ann Arbor, MI, USA; <sup>11</sup>Department of Pharmacy and Pharmaceutical Sciences, St Jude Children's Research Hospital, Memphis, TN, <sup>13</sup>Department of

Hematopoietic stem cell MYB enhancer in T-ALL

Pediatrics, Children's Hospital of Philadelphia, Philadelphia, PA; <sup>14</sup>Gilbert S. Omenn Department of Computational Medicine and Bioinformatics, University of Michigan, Ann Arbor, MI, USA. \*Co-first authors. <sup>15</sup>Co-corresponding authors.

Correspondence:

Russell J.H. Ryan

1500 E Medical Center Drive

Ann Arbor, MI 48109-5936

rjhryan@med.umich.edu

Tel: 734-647-6768

Mark Y. Chiang

109 Zina Pitcher Place

Ann Arbor, MI 48109-2200

markchia@umich.edu

Tel: 734-615-7513

Text word count: 11,330 words (entire word document)

Abstract word count: 200/200

Numbers of figures: 8

Number of tables: 0

Number of references: 108

Running title: Hematopoietic stem cell MYB enhancer in T-ALL

#### **Abstract**

There is an urgent need to find targeted agents for T-cell acute lymphoblastic leukemia (T-ALL). *NOTCH1* is the most frequently mutated oncogene in T-ALL, but clinical trials showed that pan-Notch inhibitors caused dose-limiting toxicities. Thus, we shifted our focus to ETS1, which is one of the transcription factors that most frequently co-bind Notch-occupied regulatory elements in the T-ALL context. To identify the most essential enhancers, we performed a genome-wide CRISPR interference screen of the strongest ETS1-dependent regulatory elements. The #1-ranked element is located in an intron of *AHI1* that interacts with the MYB promoter and is amplified with *MYB* in ~8.5% of T-ALL patients. Using mouse models, we showed that this enhancer promotes self-renewal of hematopoietic stem cells and T-cell leukemogenesis, maintains early T-cell precursors, and restrains myeloid expansion with aging. We named this enhancer the hematopoietic stem cell MYB enhancer (H-Me). The H-Me shows limited activity and function in committed T-cell progenitors but is accessed during leukemogenesis. In one T-ALL context, ETS1 binds the ETS motif in the H-Me to recruit cBAF to promote chromatin accessibility and activation. ETS1 or cBAF degraders impaired H-Me function. Thus, we identified a targetable stem cell element that is co-opted for T-cell transformation.

#### Introduction

The discovery of Notch-activated tumors, including ~60% of cases of T-ALL, spurred excitement to clinically test pan-Notch inhibitors, such as gamma-secretase inhibitors (GSIs), for the treatment of human cancers (1-3). Unfortunately, early clinical studies reported excessive toxicities with continuous GSI dosing (4-6). GSI toxicities result from abrogation of Notch signals crucial for normal homeostasis, particularly in the intestine (7-9). Proteomic, transcriptional genomic, and biochemical studies show that the core Notch/RBPJ complex can interact with context-dependent transcriptional regulators that co-bind its response elements (10-21). Other regulators also bind near Notch at these elements (15, 22-25). If T-lineage regulators are hijacked to drive Notch-activated T-ALL, then inhibiting them might oppose oncogenic Notch signals while circumventing the toxicities of systemic Notch inhibition. Among these factors, we prioritize ETS1 (26-28). At Notch-bound regulatory elements, we and others showed that ETS is the #1 or #2 ranked non-RBPJ motif in T-ALL in both frequency and statistical significance (21, 29). Our groups also showed that ETS1 overlaps strikingly high% (76-82%) of Notch/RBPJ-occupied elements (21, 30), more than any other transcription factor tested. Further, an ETS1 inhibitor is predicted to be safer than GSI given that postnatal ETS1 expression is highest in the thymus and other lymphoid sites relative to other tissues (31) (Figure S1A). In contrast, Notch receptor expression shows low tissue specificity (Figure S1B-E). Accordingly, we previously showed that Ets1 deprivation in mice suppresses Notch-induced target genes, thymopoiesis and leukemogenesis like GSI but had no significant effects on overall health (21).

Because of above reasons, we shifted our focus from Notch to ETS1. Here, we sought to identify the ETS1-dependent network of essential regulatory elements through a genome-wide CRISPR interference (CRISPRi) screen. Our study identified a long-range Notch and ETS1-bound MYB enhancer as the top-ranked essential element; established the important physiological role of this

element in hematopoietic stem cells and early T-cell progenitors (ETPs); determined the essential oncogenic role of this element for T-cell leukemogenesis; showed the dependence of this element on ETS1 for chromatin accessibility and activity in one T-ALL context; and highlighted SWI/SNF and ETS1 degradation but not Notch inhibition as approaches that might target this element among multiple other effects.

#### Results

Genome-wide CRISPR-interference essentiality screen of ETS1-dependent regulatory elements nominates the +140kb MYB enhancer as the most essential element

To assess downstream mechanisms of ETS1, we aimed to characterize the ETS1 "essential regulome" through a high throughput DOX-inducible CRISPRi essentiality screen. CRISPRi is the preferred screening methodology to identify essential regulatory elements (32). We first used our previously published H3K27Ac ChIP-seq and ATAC-seq datasets in THP-6 cells (21) and an activity model (33) to predict highly active T-ALL regulatory elements (Figure 1A). Next, we intersected these elements with "dynamic" ETS1 peaks, which we defined as ETS1 peaks that give decreased H3K27Ac and ETS1 ChIP-seg signal upon ETS1 knockdown in THP-6 cells (21). Lastly, we intersected these elements with strong H3K27Ac ChIP-seq peaks in primary T-ALL samples (Blueprint) to identify 1,433 candidate ETS1-dependent regulatory elements. We then transduced THP-6 cells with a custom ~30K sqRNA library targeting these elements (mean 20 sgRNAs/kb). MAGeCK analysis on paired T0 and T15 datasets (N=3) identified 10 essential elements that were as negatively selected as 39 positive control promoters of pan-essential genes (Figure 1B). The #2 and #3-ranked elements were the previously reported Notch-dependent MYC enhancer ("N-Me") (34, 35) and the BCL11B enhancer ("ThymoD") respectively (36, 37), thus validating our screen. WGS analysis of THP-6 cells revealed a structural variant involving ThymoD and the NKX2-5 oncogene (Figure S2A), similar to previous reports (38-40), that led to NKX2-5 overexpression (Figure S2B). Further WGS and STR analysis showed that THP-6 cells and CEM-CCRF cells are genetically divergent with a common origin. The #1-ranked element was an enhancer that lies +140kb from the MYB TSS and within Intron 23 of AHI1. MYB is a highly expressed oncogene across all T-ALL subgroups (41). This element was previously identified as a highly conserved enhancer ("MYB-enh-3") in erythroid leukemia cells that shows correlation between MYB expression and chromatin accessibility in human blood cells (42). This enhancer is an ETS1-dependent super-enhancer and makes long-range contacts with *MYB* in T-ALL cells (Figure S3A-B) (21).

The +140kb element is a hematopoietic stem cell (HSC) MYB enhancer (H-Me) that appears relatively quiescent in the developmental stages from which T-ALL initiates.

Publicly available ATAC-seq data in sorted murine cells show that accessibility of the +140kb element is high in long term hematopoietic stem cells (LT-HSCs) but quickly begins to fall in short-term HSCs and reduces to baseline at the DN4 stage (Figure 1C). Thus, we presumptively named this element "H-Me" for hematopoietic stem cell MYB enhancer (H-Me). In human cells, the chromatin is accessible in hematopoietic progenitor cells through DN3/DN4 cells and then goes down to baseline at the ISP stage (Figure 1D). However, despite being accessible, H3K27ac profiling shows that enhancer activity drops considerably at the DN3/DN4 stage (Figure 1E). Histone profiling of human DP thymocytes suggests that the H-Me does not acquire H3K27me3 upon further differentiation (Figure 1F). These data suggest that compared to stem cells, the H-Me is less accessible or active in immature T cells (DN3-to-ISPs) but is "primed" for reactivation. Thus, T-ALL cells do not necessarily use active enhancers native to their developmental stage during oncogenesis.

## The H-Me restricts HSC numbers and maintains ETPs, but has limited function after T-cell commitment

To investigate the function of the H-Me, we generated H-Me conditional knockout mice (*H-Me<sup>ff</sup>*). These mice contain loxP sites flanking the H-Me element, a 369-bp nucleosome-free region homologous to the human H-Me (Figure 2A). We crossed these mice with *Mx1Cre* transgenic mice (48) to generate *Mx1Cre H-Me<sup>ff</sup>* mice and littermate *Mx1Cre controls*. To delete the H-Me in HSCs, we injected 4-6-week-old mice with pl-pC. At 6 weeks, we observed efficient H-Me deletion (Figure S4A) and ~61% reduction in *Myb* expression in sorted HSCs (Figure 2B). In

contrast, we saw no statistically significant effects on *Ahi1* expression or in hematopoietic stem and progenitor cells (LSK cells, Figure S4B). H-Me deletion led to a ~2.1-fold increase in long-term HSC numbers (Figure 2C-D).

In contrast to HSCs, no effects were observed in LSKs (Figure 2E), MPP/ST-HSCs (Figure 2F), or lymphoid-primed multipotent progenitor cells (LMPP, Figure 2G). In the thymus, we observed a ~5.5-fold reduction in early T-cell precursors (ETPs, Figure 2H-I); no effects on DN2a (Figure 2J) and DN2b (Figure 2K) cells; ~2-fold reduction in T-committed DN3 (Figure 2L) and DN4 (Figure 2M) cells; and no effect on more differentiated thymocytes (Figure S4C-G) or total thymocytes (Figure S4H). H-Me deletion did not affect numbers of bone marrow myeloid/erythroid progenitors; total bone marrow cells; peripheral myeloid and lymphoid cells; or peripheral blood counts (Figure S4I-W). These data suggest that the H-Me has important roles in restricting HSC population growth and in maintaining ETPs. However, there are relatively modest effects, if any, on other cell types.

Next, we crossed *H-Me<sup>f/f</sup>* mice with *II7rCre* transgenic mice (49), which is lymphoid-specific, to generate *II7rCre H-Me<sup>f/f</sup>* mice and *II7rCre* littermate controls. We observed efficient deletion of the H-Me in the thymus (Figure S5A). *Myb* expression decreased ~50% in ETPs but was restored in subsequent stages (Figure 2N). *Ahi1* expression was not affected (Figure S5B). Consistent with the effects on *Myb* expression, H-Me deletion reduced ETPs by ~3.4-fold (Figure S5C-D) but had no statistically significant effect on subsequent stages (Figure S5E-O). These data suggest that the H-Me has ETP stage-restricted effects in maintaining cell number and *Myb* expression during thymopoiesis.

Under stress conditions, the H-Me is important for long-term HSC self-renewal but not for primary engraftment

We wondered whether the increased numbers of phenotypically defined HSCs in *Mx1Cre H-Me*<sup>A/A</sup> mice might herald eventual depletion of LT-HSC capacity as a consequence of non-self-renewing divisions. To test this possibility, we performed serial competitive bone marrow transplant (BMT, Figure 3A). We observed modest, if any, change in primary reconstitution of peripheral blood compartments after the first BMT (Figure 3B-E). However, after the second BMT, H-Me deletion gave significant loss in reconstitution of peripheral blood compartments (Figure 3F-I). Consistently, we observed no effect of H-Me deletion on reconstitution of the HSC or MPP compartments after the first BMT (Figure S6A-C) but saw significantly impaired HSC reconstitution after the second BMT (Figure 3J-K). Total MPP was not affected (Figure 3L). Similarly, in the thymus, *H-Me* deletion modestly reduced reconstitution after the first BMT (Figure S6D), but strongly impaired reconstitution after the second transplant (Figure S6E). These data suggest that under stress conditions, the H-Me is important for long-term HSC self-renewal but has relatively modest, if any, effects on primary engraftment of stem cell and thymopoietic compartments.

#### The floxed H-Me is a hypomorphic enhancer

The introduction of a LoxP sites might affect expression of the three genes in the TAD (*Hbs1l*, *Myb*, and *Ahi1*). To address this, we measured *Hbs1l*, *Myb*, and *Ahi1* expression in HSCs and ETPs from 5-8-week-old wildtype control and *H-Me<sup>ff</sup>* mice. *H-Me<sup>ff</sup>* HSCs showed reduced *Myb* expression compared to controls (Figure S7A). *Ahi1* and *Hbs1l* were modestly or not significantly affected (Figure S7B-C). *H-Me<sup>ff</sup>* ETPs showed reduced *Myb* expression compared to controls (Figure S7D). *Ahi1* and *Hbs1l* were not significantly affected (Figure S7E-F). We also observed a non-significant increase in HSCs (Figure S7G-H) and a decrease in ETPs (Figure S7I-J) in *H-Me<sup>ff</sup>* mice. The effect sizes of the floxed H-Me on *Myb* expression and HSC/ETP numbers were smaller than the effect sizes of H-Me deletion (Figure 2B, 2D, 2l, S5B, S5D). Taken together, these data suggest that the floxed H-Me is a hypomorphic Myb enhancer. These data show a

limitation of the mouse model and raise the importance of transplantation experiments for ruling out cell non-autonomous effects.

#### The H-Me limits myeloid expansion and HSC loss with aging

To understand possible toxicities of systemic H-Me inhibition, we compared H3K27ac signals in a variety of tissues in ENCODE (Figure S8A). H3K27ac signals at the H-Me were relatively strong in T-ALL cell lines and primary tumors, moderate in erythroid/B-cell derived cells and undetectable in non-blood cells. Based on these profiles, we predicted that systemic H-Me inactivation would be tolerable and avoid the toxicities of Notch inhibition. To test this, we bred *H-Me<sup>f/f</sup>* mice with Rosa26CreER<sup>T2</sup> mice. The progeny spontaneously recombined the floxed H-Me and were intercrossed to generate germline *H-Me*<sup>-/-</sup> mice. Next, we observed H-Me-deficient and littermate control mice from birth to 12 months of age. Initially, these mice showed no differences in weight up to 6 months of age. Afterwards, H-Me-deficient mice showed 6-10% reductions in weight that were stable over several months (Figure S8B). Importantly, overall survival was not affected (Figure S8C). Since our serial transplant studies revealed the importance of the H-Me for longterm HSC self-renewal, we wondered whether H-Me inactivation might cause long-term hematopoietic toxicity. At 8-months of age, peripheral blood analysis showed no differences (Figure 4A-E). However, at 12-months of age, WBC, neutrophil, and monocyte counts were increased 1.3-fold, 1.3-fold, and 2.1-fold respectively while platelet counts were mildly decreased (Figure 4F-J). In the BM, long-term HSCs were depleted 7.2-fold while MPP/ST-HSCs were depleted 2.8-fold (Figure 4K-O). In the thymus, ETPs were severely depleted 9.1-fold (Figure 4P-Q) while more differentiated populations and total thymocytes decreased by 1.9-8.6-fold (Figure 4R-U) and 2.2-fold (Figure 4V) respectively. These data suggest that the H-Me is important for maintaining HSCs and thymopoiesis and restraining myeloid cell expansion with aging.

#### Effects of H-Me deletion on HSPCs at steady state

To examine the cell cycle status of *H-Me*--- HSPCs as compared to wildtype at steady state, 10-13-week-old mice were injected with EdU followed by a 3-day maintenance period with EdU-containing water. We chose the 10-13-week-old age range in order to reliably analyze adult LT-HSCs at steady state. No difference was observed between groups with respect to EdU uptake in the LSK or LT-HSC populations (Figure S9A-B). Further, Ki67 staining showed no differences in LSK or LT-HSC cells in the G0, G1, or S-G2-M phases of the cell cycle (Figure S9C-D). These data suggest that cell cycle dynamics were unchanged in adult *H-Me*--- HSPCs as compared to *H-Me*---- at steady state.

To determine if H-Me deficiency leads to changes in the progenitor cell populations at steady state, we enumerated HSCs and MPPs (50). This staining protocol fractionates MPPs into MPP1 (CD229 CD244; with balanced lymphoid and myeloid potential, MPP2 (CD229 CD244), MPP3 (CD229 CD244; a myeloid-biased subpopulation), and a poorly characterized MPP other population (Figure S10A) (51). At 10-13 weeks of age, there were no differences in the overall cellularity of the bone marrow (Figure S10B). However, there was a non-significant 1.9-fold increase in HSCs (Figure S10C), which aligns with the HSC expansion seen at an earlier time point (Figure 2D). We did not observe any differences between control and H-Me knockout mice in the total MPP, LSK, and individual MPP populations (Figure S10D-H). However, we observed a trend towards increased cell number and relative expansion of the myeloid-biased MPP3 population compared to other MPPs (Figure S10H-I). These data are consistent with the eventual myeloid expansion seen in aged H-Me-deficient mice (Figure 4F-H). These data suggest that at steady state, the HSC expansion seen acutely after H-Me deletion has weakened and there are hints of the myeloid bias seen later in life.

#### Effects of H-Me deletion on intestinal morphology

Given the weight loss of H-Me-deficient mice over time and given the importance of *Myb* and *Ets1* for intestinal homeostasis (21, 52-56), we compared intestinal tissue in the above 10-13-week-old H-Me deficient mice compared to *H-Me*<sup>+/+</sup> control mice. Overall morphology of the intestinal tissue was not changed as visualized by H&E staining (Figure S11A) or PAS/AB staining of mucous cells (Figure S11B).

#### The H-Me is important for murine Notch-activated T-ALL leukemogenesis

Since the H-Me seemed less accessible, active, and functional in early T-committed thymocytes compared to more primitive ancestors, we wondered whether H-Me activity is increased during transformation to drive T-ALL initiation. To test this possibility, we used a well-established murine model of Notch-induced T-ALL (57, 58). We transduced bone marrow stem and progenitor cells from *H-Me*<sup>-/-</sup> mice with an activated *Notch1* allele ( $\triangle E/Notch1$ ) (59, 60) and transplanted these cells into recipient mice to generate T-ALL (Figure 5A). H-Me-deleted mice generated ~38-fold fewer peripheral T-ALL blasts (Figure 5B-C) and showed significantly prolonged survival (Figure 5D) relative to littermate control mice.

To further test whether the H-Me is important for T-ALL leukemogenesis, we transduced bone marrow stem and progenitor cells from  $Mx1Cre\ H-Me^{t/t}$  mice with  $\Delta E/Notch1$ , transplanted these cells into recipient mice, and injected pl-pC at Week 5 (Figure 5E). H-Me deletion induced a ~105-fold reduction in peripheral T-ALL blasts (Figure 5F-G) and significantly prolonged survival (Figure 5H) relative to Mx1Cre littermate control mice. Further, H-Me deletion significantly impaired leukemogenesis in a second Notch-activated T-ALL mouse model (Lmo2-tg) that is induced by an LMO2 transgene in which activating Notch1 mutations are acquired (Figure 5I-J) (61). These data suggest that the H-Me is important for murine Notch-activated T-ALL leukemogenesis.

#### The H-Me is frequently co-amplified with MYB in human T-ALL patients

Previous studies showed that the *MYB-AHI1* region is a frequent target of tandem duplications in ~8%-40% of pediatric T-ALL patient samples (62-66). Thus, we wondered whether there is positive selection for including the H-Me in these duplications in human T-ALL patients. Consistently, WGS analysis in 1,309 T-ALL samples from the Children's Oncology Group clinical trial AALL0434 (40) showed that 8.8% of patients had *MYB* amplifications, of which 97% involved the H-Me (Figure 6A). The genomic segment extending from the *MYB* gene to the H-Me appears to be a minimally amplified region. Further, ~50% of cell lines were found to carry *MYB* duplications, such as CEM cells (63). Consistently, WGS analysis showed that THP-6 cells contain MYB/H-ME duplications and is thus a clinically relevant model (Figure 6B). WGS confirmed duplication in CEM cells but did not detect it in other T-ALL cell lines used in this study (see below) (Figure 6C). These data support the importance of the H-Me in human T-ALL patients and solves the puzzling mystery of why *MYB* duplications nearly always contain part of the *AHI1* gene.

#### The H-Me is important for human T-ALL maintenance

Within the topologically associating domain (TAD) that contains *MYB*, ATAC-seq of T-ALL cell lines and primary samples showed that the H-Me ranked amongst the strongest nucleosome-free signal, stronger than previously identified *MYB* enhancers in T-ALL (67-69) (Enhancers "A" and "B" in Figure 7A). To test the importance of the H-Me, we transduced H-Me sgRNAs and dCas9-KRAB into T-ALL cell lines that represent genomically defined subtypes (40) expressing a range of *MYB* levels in *ETS1*-enriched T-ALL (Figure S12). We selected several *NOTCH1*-mutated cell lines -- THP-6 (NKX2-5), Jurkat (TAL1 (67)), MOLT14 (STAG2/LMO2 (70)), CEM (NKX2-5 (39), related to THP-6), SUP-T1 (TAL1-negative NOTCH1 t(7;9) otherwise not classified (71, 72)) and MOLT4 (TAL1 (73)) -- as well as one *NOTCH1*-wildtype cell line HSB2 (TAL1 (74)). The H-Me sgRNAs repressed expression of *MYB* by 1.3-fold to 5.5-fold (Figure 7B-D, S13A-D) and impaired

cell growth by 1.6-fold to 113-fold (Figure 7E-G, S13E-H)). MOLT4 cells appeared to be MYB-independent as MYB promoter guides suppressed *MYB* expression but not growth. To rule out non-MYB effects of the H-Me, we ectopically expressed *Myb* and then transduced sgH-Me. Enforced *Myb* expression rescued growth of H-Me repressed cells (Figure S13I-J). To test the importance of the H-Me in vivo we injected NSG mice with doxycycline-inducible dCas9-KRAB-expressing CEM cells transduced with sgRNA and then treated the mice with doxycycline. At 4 weeks, sgH-Me repressed peripheral blood blast count by 5-fold (Figure 7H-I) and significantly extended survival (Figure 7J). These effects were just as strong as repressing a pan-essential gene. Taken together, these data show that the H-Me has limited function in normal T-lineage committed progenitors but rises in importance for malignant transformation, induction of *MYB*, and maintenance of T-ALL cells without compensation by other *MYB* enhancers.

### The ETS motif in the H-Me is primarily bound by ETS1 and is important for H-Me activity in one T-ALL context

To better understand how ETS1 regulates the H-Me, we first generated THP-6 and CEM (related to THP-6) cell lines in which ETS1 was fused to FKBP<sup>F36V</sup>. Adding dTAG<sup>V</sup>-1 robustly degraded ETS1 protein, resulting in suppression of *MYB* protein and reduction of *MYB* RNA by ~4.1-fold in THP-6 cells (Figure 8A-B) and ~2.3-fold in CEM cells (Figure S14A-B). Next, we performed HOMER analysis of the H-Me across several species, which revealed strong conservation of several transcription factor motifs including a single ETS motif (Figure S15). Human-to-mouse conservation at the H-Me was high at 93% compared to just 12-15% in introns overall (75-77). To test whether ETS1 bound this motif, we performed an assay, termed "reverse ChIP", which was originally developed by the Pimanda lab (78). In this assay, nuclear extracts are incubated with a biotinylated 254bp H-Me DNA fragment containing wildtype ETS motif (AGAGGAAGTG) or mutated ETS motif (AGAGAAATG, full sequence in Figure S16A). The mutant DNA fragment pulled down less ETS1 in THP-6, CEM, and Jurkat T-ALL cells compared to wildtype control

(Figure 8C-D, S16B-E). Next, we performed mass spectrometry of "reverse ChIP" pulldowns. As a pulldown assay, this assay could in theory detect closely related ETS factors. However, ETS1 was the only protein that was differentially pulled down by wildtype compared to mutated DNA fragment by two statistical methods (Figure 8E). As a complementary approach, we attempted to generate a mutant THP-6 ETS1-FKBP<sup>F36V</sup> clone with homozygous deleted ETS binding sites. We observed strong selection against creating this clone but eventually created one clone with homozygous partial mutations (Figure 8F). ChIP showed undetectable ETS1 occupancy at the mutant H-Me relative to wildtype control (Figure 8G). These data suggest that ETS1 binds the endogenous ETS site in the H-Me.

Next, we wondered whether the ETS site in the H-Me is functional. To test this, we measured MYB mRNA in wildtype and ETS-mutant cells with or without ETS1 degradation using dTAG. Consistently, MYB expression was ~60% reduced in mutant cells compared to wildtype control (Figure 8H). Further, ETS1 degradation reduced MYB expression in wildtype control but had no effect in the mutant clone. The lack of MYB-responsiveness to ETS1 degradation is not due to clone-specific damage to ETS1-FKBP<sup>F36V</sup> functionality as dTAG treatment reduced the ETS1 target genes LYL1 and HHEX (21) (Figure S16F-G). As an orthogonal approach, we developed an H-Me luciferase reporter assay, which showed that the H-Me was active in T-ALL cells but not in U2OS or 293T cells (Figure S16H). Mutating the ETS motif (Figure S16I) or ETS1 knockdown (Figure S16J) impaired H-Me reporter activity. Although Notch/RBPJ bound the H-Me with gamma-secretase dependence (Figure S3A) (21), Notch inhibition with GSI did not impair H-Me activity (Figure S16K). These data are consistent with multiple public RNA-seq datasets showing that Notch does not generally regulate MYB (Figure S16L) (30, 84, 85). Thus, Notch appears to defer to ETS1 to induce MYB directly through the ETS site in the H-Me in one T-ALL context.

#### The SWI/SNF complex is a top-ranked candidate ETS1 cofactor at the H-Me

Since enhancers are difficult to target, we sought to identify ETS1-bound cofactors at the H-Me. Initially, we examined our H-Me "reverse ChIP" mass spectrometry data and identified 71 transcriptional regulators that differentially bound wildtype H-Me bait compared to bead controls (Figure S17A-B), including several DNA-binding sequence-specific transcription factors (Figure S17C). Next, we transduced CEM cells with Flag-ETS1 and performed anti-Flag coimmunoprecipitation followed by mass spectrometry. We identified 60 transcriptional regulators that differentially bound Flag-ETS1 compared to vector control (Figure S17D-E), including known partners RUNX1 and its cofactor CBFB (86) (Figure S17F). Finally, we intersected the H-Meinteracting proteins with the ETS1-interacting proteins to identify 13 proteins common to both groups and ranked them by strength of binding to ETS1 (Figure 8I). The top two proteins were RUNX1 and CBFB. The third ranked protein was SMARCC1, which is a subunit of SWI/SNF complexes (Figure S17C, blue dot). In addition to SMARCC1, 6 other SWI/SNF subunits differentially bound ETS1 (Figure S17D, yellow cluster; Figure S17F, blue dots). Co-IP confirmed the interaction between Flag-ETS1 and endogenous SWI/SNF subunits SMARCC1 and SMARCB1 (Figure 8J). Reciprocal co-IP confirmed the interaction between endogenous SMARCC1 and ETS1 (Figure 8K). These data suggest that SWI/SNF complexes might be recruited by ETS1 to activate the H-Me.

ETS1 recruits the cBAF complex to remodel chromatin at the H-Me in one T-ALL context

To test whether ETS1 recruits SWI/SNF to the H-Me, we degraded ETS1 in THP-6 cells and
performed ChIP for SMARCC1 at the H-Me. Consistently, ETS1 degradation reduced SMARCC1
occupancy by ~2.5-fold in THP-6 cells (Figure S18A) and ~1.6-fold in CEM cells (related to THP-6, Figure S18B). ETS1 degradation reduced H3K27ac by ~3.2-fold at the H-Me (Figure S18C).
ETS1 degradation reduced ARID1A signals (specific for cBAF) by ~2.3-fold but had no effect on
PBRM1 occupancy (specific for PBAF) at the H-Me (Figure 8L). Next, we performed ATAC-seq.
ETS1 degradation strongly reduced H-Me chromatin accessibility by ~4.9-fold at FDR<6.8E-15

(Figure 8M). Next, we wondered whether the ETS motif in the H-Me is required for SWI/SNF function. To test this, we measured *MYB* mRNA in the ETS-mutant cells (Figure 8F) after SWI/SNF degradation with AU-15330. Consistently, SWI/SNF degradation reduced *MYB* expression in ETS-mutant cells by only ~20% in contrast to ~80% in control cells (Figure 8N). The lack of *MYB*-responsiveness to SWI/SNF degradation was not due to clone-specific damage as AU-15330 treatment strongly repressed the ETS1 target genes *LYL1* and *HHEX* (21) in this clone (Figure S18D-E). These data suggest that ETS1 recruits the cBAF complex to the H-Me to promote chromatin accessibility and *MYB* induction in one T-ALL context.

#### cBAF inhibitors inactivate the H-Me and downregulate MYB in two T-ALL contexts

The above data raised the possibility that proteolysis-targeting chimera (PROTAC) degraders of SMARCA2/4, such as ACBI1 (87) and AU-15330 (88), might be effective in targeting the H-Me. To test this, we generated dose-response curves with these compounds on CEM, Jurkat, and THP-6 cells. All three cell lines showed <100nM sensitivity to AU-15330, which classifies them as "sensitive" (Figure S19A) (88). Jurkat and THP-6 cells, but not CEM cells, were also sensitive to ACBI1 (Figure S19B). To test whether SMARCA2/4 degradation inactivates the H-Me, we performed H3K27ac gChIP. AU-15330 treatment reduced H3K27ac signals by ~11.1-fold in THP-6 cells (Figure S19C) and ~2.1-fold in CEM cells (Figure S19D). Consistently, AU-15330 suppressed MYB transcripts by ~1.3-4-fold (Figure S19E-G) and MYB protein levels by ~2.3-9.7fold (Figure 8O, S20A). ACBI1 failed to degrade SMARCA2/4 protein levels in CEM cells (Figure S20B), which is consistent with its weak growth inhibitory effects and lack of effect on MYB transcripts (Figure S20C) and protein (Figure S20B) in these cells. In contrast, ACBI1 suppressed MYB transcripts by ~1.4 and ~2-fold and MYB protein by ~7 and ~25-fold in Jurkat and THP-6 cells respectively. These data suggest that SMARCA2/4 degradation might be an effective strategy for inhibiting H-Me activity and MYB expression, among multiple other effects (89), in two T-ALL contexts.

#### **Discussion**

While many T-ALL-associated transcriptional regulators have been identified, there remains limited understanding of the non-coding elements at which these factors assemble and coordinate in hierarchies to promote oncogenesis. Despite important work in this area (22, 67, 68, 90-92), there are knowledge gaps, particularly in identifying the most important oncogenic enhancers and finding ways to safely eject transcription factors bound to these elements as potential therapeutic strategies. To help close these knowledge gaps, we performed an unbiased essentiality screen of regulatory elements that bind ETS1 and are dependent on ETS1 for H3K27ac modification in the Notch-activated THP-6 cell line. Our screen showed that the most essential ETS1-dependent element was the H-Me, a Notch-independent superenhancer that induces *MYB*. In T-ALL, supraphysiological MYB activity can be induced through translocations, tandem duplications, and genetic variants conferring increased protein stability; however, most T-ALL tumors (~83-95%) have no known *MYB* genetic lesion (62-68, 93). Thus, native elements like the H-Me are likely important drivers of MYB expression in most cases, including tandem duplications since they nearly always amplify the H-Me. Our screen also showed that the second most essential element was the Notch-dependent MYC enhancer (N-Me) (34, 35).

Although the H-Me and the N-Me share similarities as developmental enhancers that are co-opted to promote T-ALL oncogenesis, they confer different stage-specific dependences. The marked T-cell developmental defects in *LckCre Myc*<sup>4/4</sup> mice phenocopy the marked defects in N-Me deficient mice (34). In contrast, the marked T-cell developmental defects in *LckCre Myb*<sup>4/4</sup> mice (94) are not seen in H-Me deficient mice. These phenotypic differences might be explained by the disparate chromatin configurations of these enhancers in DN3/pre-T cells when *LckCre* initially becomes active (95). While N-Me accessibility peaks at DN3/DN4 (22), H-Me accessibility peaks

developmentally earlier in primitive HSCs. While the N-Me shows high H3K27ac signals in DN3/DN4 cells, the H-Me shows low H3K27ac signals (Figure 1E). Hence, it is not surprising that N-Me deletion caused marked T-cell developmental defects whereas H-Me deletion did not. We and others previously showed that DN3, DN4, or ISP cells are highly enriched for leukemia-initiating cells, depending on the T-ALL mouse model (43-45) and similar to human T-ALL (47). Thus, the N-Me appears to be fully accessible to immature T cells as they transform to T-ALL. In contrast, it is not apparent how developing T-ALL cells can easily access the oncogenic potential of the H-Me. These cells presumably restructure the H-Me to a more open configuration or aberrantly sustain the stem cell configuration during T-cell differentiation in order to hijack this stem cell element to drive oncogenesis. Emerging evidence suggests that developmental T-ALL enhancers can be separated into thymocyte-active elements (e.g. *Myc* and *Pten*) and stem cell-active elements (e.g. *Myb* and *Mycn*) (34, 35, 96, 97).

Myb deletion and H-Me deletion show similarities and differences. Conditional Myb deletion using Mx1Cre led to dramatic reductions in HSCs, MPPs, myeloid progenitors and differentiated blood populations (98). In contrast, conditional H-Me deletion using Mx1Cre acutely led to an increase in HSCs and no statistically significant effects on MPPs, myeloid progenitors, or differentiated blood populations. Later, between intermediate and aged time points, the H-Me-deficient HSC expansion wanes and then reverses to HSC depletion with evolving relative and/or absolute myeloid expansion, particularly monocytosis. The H-Me-deficient HSC and monocyte phenotypes are similar to what has been reported comparing 2-month-old and 12-month-old  $Myb^{+/-}$  mice (99). Induction of Myb haploinsufficiency leads to time-dependent accumulation of myeloid proliferation disease by 22 months of age (99). Germline Myb deletion is embryonic lethal due to severe anemia (100) while germline H-Me-deleted mice have normal survival with normal blood counts and weights up until 6-8 months. A single competitive bone marrow transplant of conditional Myb-deleted or  $Myb^{+/-}$  bone marrow revealed impaired HSC self-renewal or reconstitution (98, 99).

However, conditional H-Me-deficient mice required serial competitive bone marrow transplants to reveal impaired HSC self-renewal or reconstitution. *Myb* deletion using *LckCre* led to ~10-fold loss in thymus cellularity, particularly at the DP thymocyte stage (94). In contrast, conditional H-Me deletion using *Mx1Cre* or *II7rCre* caused stage-restricted ETP loss during thymopoiesis. Taken together, H-Me deletion has milder and/or stage-restricted effects compared to *Myb* deletion. While these data highlight an example of theoretical safety advantage of enhancer targeting over gene targeting, they also show that enhancer targeting would still have important ramifications, particularly in old age.

We are mindful that the H-Me is a single enhancer within a large transcriptional hub (Figure S3A). Thus, it is possible that deletion of the H-Me or insertion of the LoxP sites might affect other Myb regulatory elements in the TAD. Insertion of the LoxP sites also creates a hypomorphic H-Me enhancer. This is an important limitation of our floxed mouse model although the conclusions of this manuscript are based on comparisons between  $H-Me^{+/+}$  and  $H-Me^{A/A}$  mice as well as orthogonal models, such as germline H-Me knockout mice and human T-ALL cell lines.

The literature is replete with examples of Notch signaling being central to T-ALL oncogenesis (3). However, we here highlight a contrasting example of a top oncogenic element where Notch is not dominant, instead deferring to ETS1. The reason for why NOTCH1 binds the H-Me is unclear. It is possible that NOTCH1 induced H-Me activity early during leukemogenesis, but subsequent compensatory Notch-independent signals later converged on the H-Me, rendering Notch occupancy dispensable. Consistently, HSB2 cells, which lack *NOTCH1* mutations, require Notch-independent signals at the H-Me for population cell growth. Mechanistically, ETS1 appears particularly important since it binds and recruits the cBAF complex to the ETS site to promote accessibility and induce *MYB* in THP-6/CEM cells. Since open chromatin is required for transcription factor binding, the chromatin remodeling function of ETS1 likely explains our

previous observations that *ETS1* knockdown reduced Notch and Notch cofactor occupancy at a subset of ETS1-bound enhancers (21) (Figure S20D).

The importance of SWI/SNF and ETS1 occupancy at the H-Me might have therapeutic implications. Consistently, SMARCA2/4 and ETS1 degradation inactivated the H-Me, resulting in downregulation of MYB. The resultant growth inhibitory effects are consistent with recent reports that cBAF is important for promoting chromatin accessibility and transcriptional activity of RUNX1/CBFB, which are the top ETS1 interaction partners in our screen (Figure 8I) (89, 101). While these findings are promising, there are some limitations. First, we caution that the details of how ETS1 activates the H-Me and MYB has not been tested in all T-ALL contexts. Second, our H-Me ETS motif knockout reporter assay showed expected loss of gene activation; and while reporter assays are statistically predictive of true regulatory activity in high-throughput assays (79-83), effects of individual reporter constructs may not always recapitulate all regulatory effects in situ. While we were able to generate a THP-6 clone with homozygous H-Me mutations that led to loss of ETS1 binding and regulatory effects on MYB, we were unable to derive clones with homozygous loss of the core ETS motif, possibly due to strong negative fitness effects. Third, since transcriptional regulators like ETS1 and cBAF are not specific to MYB or the H-Me but regulate thousands of target genes, inhibiting them might not be safe in humans. (21, 89). Fourth, our study does not offer a unique mechanism or strategy to target a single gene out of thousands of genes or a single enhancer out of thousands of enhancers. Despite these limitations, given the safety of ubiquitous Ets1 deletion in mice (21) and since SWI/SNF inhibitors are entering clinical trials (102), our study suggests that ETS1 and cBAF degradation are reasonable therapeutic strategies to test in human T-ALL.

#### Acknowledgements

We thank J. Douglas Engel, Yi Fang Guan, John Pimanda, Nirmalya Saha, Andrew Muntean, and Venkatesha Basrur for their thoughtful input and technical assistance during this project. We thank Abdullah Ramzan for providing code. We thank Joonsoo Kang and Hans-Reimer Rodewald for the *Il7rCre* mice. We thank Utpal Davé for the *CD2-Lmo2-tg* mice. We thank Arul Chinnaiyan for providing AU-15330 compound. This work was supported by funding from the National Institutes of Health (R01CA27611701 [M.C.]; R01Al136941 [M.Y.C.]; T32GM145470 [K.L.]; R35 CA197695 [C.G.M.], and P30 CA021765 [C.G.M.]), University of Michigan Rackham Graduate School, Michigan Medicine Rogel Cancer Center, American Lebanese Syrian Associated Charities of St. Jude Children's Research Hospital, and the Rally Foundation for Childhood Cancer Research.

#### **Authorship Contributions**

The order of the co-first authors C.M. and K.L. was established based on equal contribution. Conceptualization: M.Y.C., C.M., K.L., R.J.H.R., A.C.M (Monovich), P.P, D.T.T., C.G.M., M.C. Investigation: C.M., K.L., C.S., A.C.M. (McCarter), E.C., A.F.M, S.L., Q.W., A.I., K.B.R., M.J., K.C., T.K., P.E., A.W., J.N., S.K., Z.S. Visualization: M.Y.C., R.J.H.R., C.M., K.L., E.C., K.C., M.J., T.M.K., P.P. Formal Analysis: M.Y.C., C.M., K.L., C.S., E.C., Y.D., F.V.L., K.B.R., P.P. Data Curation: M.Y.C., C.M., K.L., D.S. Funding acquisition: M.Y.C. and C.G.M. Writing of the original draft: M.Y.C., C.M., K.L., E.C., K.C., M.J., L.C.S. Review and editing of the manuscript: C.M., K.L., C.S., A.C.M (Monovich), E.C., A.F.M, S.L., Q.W., A.I., A.C.M. (McCarter), D.T.T., C.G.M., P.P., M.C., Q.L., M.J., L.C.S., Y.D., D.S., F.V.L., A.I.N., R.J.H.R. Supervision: M.Y.C., A.I.N., D.S., D.T.T., C.G.M., R.J.H.R.

#### **Conflict-of-interest**

The authors have declared that no conflict of interest exists.

#### Methods

#### Sex as a biological variable

For developmental and gene expression analyses, mice of both sexes generated from heterozygous-to-heterozygous matings were used to generate data. These data were combined when no differences were noted. Since no differences were noted, sex was not considered as a biological variable for bone marrow transplantation experiments.

#### Mice

C57/BL6N mice between 4-8 weeks old were purchased from Taconic. 564 B6-Ly5.1/Cr mice between 4-8 weeks were purchased from Charles River Breeding Labs. Mice were backcrossed to the C57/BL6N strain at least 5 times. Mx1Cre mice were a gift from Qing Li (University of Michigan, Ann Arbor). Il7rCre mice were a gift of Hans-Reimer Rodewald (German Cancer Research Center, Heidelberg) (49). NSG mice were obtained from Jax (Strain #:005557). The conditional H-Me floxed mice were generated using Easi-CRISPR (Quadros, Genome Biology, 2017) by the University of Michigan Transgenic Animal Model Core. Briefly, ES cells were microinjected with a megamer donor containing 5' and 3' loxP sites flanked the 369bp H-Me segment (chr10:21,054,606-21,054,974; mm10), Cas9, and 5' and 3' sqRNA guides. A 47-bp rabbit beta globin splice acceptor sequence (103) was placed in the megamer donor between the 3' loxP site and Exon 20 of Ahi1. The Mx1Cre H-Me<sup>f/f</sup> and II7rCre H-Me<sup>f/f</sup> mice were generated by crossing *H-Me<sup>f/f</sup>* mice with Mx1-Cre mice and II7rCre mice respectively. Cre expression in Mx1Cre H-Me<sup>f/f</sup> mice that were 4-6 weeks of age was induced with pl-pC (Amersham, 40 ug i.p. every 2 days for 5 times) and analyzed at 6 weeks after the last injection (11-13 weeks of age). H-Me<sup>f/f</sup> mice of both sexes were analyzed at 5-8 weeks of age. II7Cre H-Me<sup>ff</sup> mice of both sexes were analyzed at 5-10 weeks of age. Germline H-Me knockout mice of

both sexes were analyzed at 10-13 weeks of age. Aged H-Me deficient mice of both sexes were analyzed at 52-54 weeks of age.

#### Constructs

Flag-ETS1 construct was generated as previously described<sup>1</sup>. H-Me<sup>WT</sup> and H-Me<sup>Mut</sup> constructs were generated by subcloning from designed gBlocks from IDT into the pGL3-luciferase-promoter vector (Promega). The TET3G activator plasmid was generated by subcloning the TET3G from pLVX-EF1a-Tet3G (Clontech #631359) into pRRLsin.cPPTCTS.MNDU3.BXE.PGK.NGFR.WPRE (gift from Andrew Weng, British Columbia Cancer Agency, Vancouver). CRISPRi sgRNAs were cloned into the sgOPTI virus (Addgene #85681; RRID:Addgene\_85681) and co-transduced with TRE-KRAB-dCas9-IRES-GFP virus (Addgene #85556; RRID:Addgene\_85556) and TET3G activator virus (104). These constructs were used for all CRISPRi experiments with the exception of CEM and THP-6 cells in Figure 3I-J, which used a constitutive CRISPRi construct, pLV-hU6-sgRNA-hUbC-dCAS9-KRAB-T2a\_puro (Addgene #71236; RRID:Addgene\_71236).

#### **Cell lines**

CEM/SS, THP-6, SUP-T1, MOLT4, and Jurkat cells were obtained and cultured as previously published (20, 21). HSB2 and MOLT14 cells were obtained from Charles Mullighan (St. Jude Children's Research Hospital, Memphis). DOX-inducible CRISPRi cell lines were generated as previously published (104). All human cell lines were authenticated using STR analysis prior to use to match an established cell line standard (DSMZ) or an internal standard when a reference is not available (THP-6) (Labcorp). All cell lines were cultured less than 3 months after resuscitation and tested for contaminants using MycoAlert (Lonza) every 1-3 months to ensure they were free of Mycoplasma contamination.

#### Antibodies, sgRNAs, HDR templates and primers

These reagents are listed in Table S1.

#### **Statistics**

Unless otherwise indicated, P-values were derived from two-sided two-sample t-tests of Log2-transformed data for comparisons in experiments involving two groups and 1-way ANOVA for pairwise contrasts in experiments with more than two groups. Unless otherwise stated, horizontal lines are means and values are shown as mean <u>+</u> standard deviation. Survival curves (or time to event data) was tested with log-rank tests comparing pairs of groups. A P value less than 0.05 was considered significant.

#### Data availability

High-throughput sequencing data, results, and statistics were deposited in the Gene Expression Omnibus database with accession number GSE263585, GSE263913, GSE263952, and GSE263977 and are publicly accessible. The publicly available NGS datasets used during the present study can be found in GEO under accession numbers: GSE225559, GSE221345, GSE151075, GSE51800, GSE29600, GSE134761, GSE94000, GSE151075, GSE29181, GSE79422, GSE117749, GSE93755, GSE138516, GSE109125, GSE22601, GSE129086, GSE110630, GSE76783, GSE90715, GSE116873, and GSE138659. H3K27ac ChIP-seq profiles of sorted thymocyte subsets were obtained from <a href="https://viz.stjude.cloud/mullighan-lab/collection/the-genomic-basis-of-childhood-t-lineageacute-lymphoblastic-leukemia~29">https://viz.stjude.cloud/mullighan-lab/collection/the-genomic-basis-of-childhood-t-lineageacute-lymphoblastic-leukemia~29</a>. BLUEPRINT project DP thymocyte histone profiles were obtained from EGAD00001002369. WGS datasets were obtained from phs002276.v2.p1, phs000218, phs000464. Supporting data values are in the XLS file, as described above.

#### References

- 1. Miele L, and Artavanis-Tsakonas S. *Targeting Notch in Cancer From the Fruit Fly to the Clinic*. Springer; 2018.
- 2. Weng AP, Ferrando AA, Lee W, Morris JPt, Silverman LB, Sanchez-Irizarry C, et al. Activating mutations of NOTCH1 in human T cell acute lymphoblastic leukemia. *Science*. 2004;306(5694):269-71.
- 3. McCarter AC, Wang Q, and Chiang M. Notch in Leukemia. *Adv Exp Med Biol.* 2018;1066:355-94.
- 4. Deangelo DJ, Stone RM, Silverman LB, Stock W, Attar EC, Fearen I, et al. A phase I clinical trial of the notch inhibitor MK-0752 in patients with T-cell acute lymphoblastic leukemia/lymphoma (T-ALL) and other leukemias *Journal of Clinical Oncology, 2006 ASCO Annual Meeting Proceedings.* 2006;24(18S):6585.
- 5. Krop I, Demuth T, Guthrie T, Wen PY, Mason WP, Chinnaiyan P, et al. Phase I pharmacologic and pharmacodynamic study of the gamma secretase (Notch) inhibitor MK-0752 in adult patients with advanced solid tumors. *J Clin Oncol.* 2012;30(19):2307-13.
- 6. Tolcher AW, Messersmith WA, Mikulski SM, Papadopoulos KP, Kwak EL, Gibbon DG, et al. Phase I study of RO4929097, a gamma secretase inhibitor of Notch signaling, in patients with refractory metastatic or locally advanced solid tumors. *J Clin Oncol*. 2012;30(19):2348-53.
- 7. van Es JH, van Gijn ME, Riccio O, van den Born M, Vooijs M, Begthel H, et al. Notch/gamma-secretase inhibition turns proliferative cells in intestinal crypts and adenomas into goblet cells. *Nature*. 2005;435(7044):959-63.
- 8. Carulli AJ, Keeley TM, Demitrack ES, Chung J, Maillard I, and Samuelson LC. Notch receptor regulation of intestinal stem cell homeostasis and crypt regeneration. *Dev Biol.* 2015;402(1):98-108.
- 9. VanDussen KL, Carulli AJ, Keeley TM, Patel SR, Puthoff BJ, Magness ST, et al. Notch signaling modulates proliferation and differentiation of intestinal crypt base columnar stem cells. *Development*. 2012;139(3):488-97.
- 10. Pinnell N, Yan R, Cho HJ, Keeley T, Murai MJ, Liu Y, et al. The PIAS-like Coactivator Zmiz1 Is a Direct and Selective Cofactor of Notch1 in T Cell Development and Leukemia. *Immunity*. 2015;43(5):870-83.
- 11. Yatim A, Benne C, Sobhian B, Laurent-Chabalier S, Deas O, Judde JG, et al. NOTCH1 nuclear interactome reveals key regulators of its transcriptional activity and oncogenic function. *Mol Cell.* 2012;48(3):445-58.
- 12. Lin S, Tian L, Shen H, Gu Y, Li JL, Chen Z, et al. DDX5 is a positive regulator of oncogenic NOTCH1 signaling in T cell acute lymphoblastic leukemia. *Oncogene*. 2013;32(40):4845-53.
- 13. Borggrefe T, and Liefke R. Fine-tuning of the intracellular canonical Notch signaling pathway. *Cell Cycle*. 2012;11(2):264-76.
- 14. Bray SJ, and Gomez-Lamarca M. Notch after cleavage. *Curr Opin Cell Biol.* 2018;51:103-9.
- 15. Pajcini KV, Xu L, Shao L, Petrovic J, Palasiewicz K, Ohtani Y, et al. MAFB enhances oncogenic Notch signaling in T cell acute lymphoblastic leukemia. *Sci Signal*. 2017;10(505).
- 16. Hein K, Mittler G, Cizelsky W, Kuhl M, Ferrante F, Liefke R, et al. Site-specific methylation of Notch1 controls the amplitude and duration of the Notch1 response. *Sci Signal*. 2015;8(369):ra30.

- 17. Yu Z, Wu H, Chen H, Wang R, Liang X, Liu J, et al. CAF-1 promotes Notch signaling through epigenetic control of target gene expression during Drosophila development. *Development*. 2013;140(17):3635-44.
- 18. Marcel N, Perumalsamy LR, Shukla SK, and Sarin A. The lysine deacetylase Sirtuin 1 modulates the localization and function of the Notch1 receptor in regulatory T cells. *Sci Signal*. 2017;10(473).
- 19. Mulligan P, Yang F, Di Stefano L, Ji JY, Ouyang J, Nishikawa JL, et al. A SIRT1-LSD1 corepressor complex regulates Notch target gene expression and development. *Mol Cell.* 2011;42(5):689-99.
- 20. Melnick AF, Mullin C, Lin K, McCarter AC, Liang S, Liu YE, et al. Cdc73 protects Notchinduced T-cell leukemia cells from DNA damage and mitochondrial stress. *Blood*. 2023;142(25):2159-74.
- 21. McCarter AM, Della Gatta G, Melnick A, Kim E, Sha C, Wang Q, et al. Combinatorial ETS1-dependent control of oncogenic NOTCH1 enhancers in T-cell leukemia. *Blood Cancer Discovery.* 2020;1(2):178-97.
- 22. Belver L, Yang AY, Albero R, Herranz D, Brundu FG, Quinn SA, et al. GATA3-Controlled Nucleosome Eviction Drives MYC Enhancer Activity in T-cell Development and Leukemia. *Cancer Discov.* 2019;9(12):1774-91.
- 23. Antoszewski M, Fournier N, Ruiz Buendia GA, Lourenco J, Liu Y, Sugrue T, et al. Tcf1 is essential for initiation of oncogenic Notch1-driven chromatin topology in T-ALL. *Blood*. 2022;139(16):2483-98.
- 24. Choi A, Illendula A, Pulikkan JA, Roderick JE, Tesell J, Yu J, et al. RUNX1 is required for oncogenic Myb and Myc enhancer activity in T cell acute lymphoblastic leukemia. *Blood*. 2017.
- 25. Jenkins CE, Gusscott S, Wong RJ, Shevchuk OO, Rana G, Giambra V, et al. RUNX1 promotes cell growth in human T-cell acute lymphoblastic leukemia by transcriptional regulation of key target genes. *Exp Hematol.* 2018;64:84-96.
- 26. Wei GH, Badis G, Berger MF, Kivioja T, Palin K, Enge M, et al. Genome-wide analysis of ETS-family DNA-binding in vitro and in vivo. *EMBO J.* 2010;29(13):2147-60.
- 27. Hollenhorst PC, McIntosh LP, and Graves BJ. Genomic and biochemical insights into the specificity of ETS transcription factors. *Annu Rev Biochem.* 2011:80:437-71.
- 28. Garrett-Sinha LA. Review of Ets1 structure, function, and roles in immunity. *Cell Mol Life Sci.* 2013;70(18):3375-90.
- 29. Wang H, Zou J, Zhao B, Johannsen E, Ashworth T, Wong H, et al. Genome-wide analysis reveals conserved and divergent features of Notch1/RBPJ binding in human and murine T-lymphoblastic leukemia cells. *Proc Natl Acad Sci U S A*. 2011;108(36):14908-13.
- 30. Wang H, Zang C, Taing L, Arnett KL, Wong YJ, Pear WS, et al. NOTCH1-RBPJ complexes drive target gene expression through dynamic interactions with superenhancers. *Proc Natl Acad Sci U S A.* 2014;111(2):705-10.
- 31. Oikawa T, and Yamada T. Molecular biology of the Ets family of transcription factors. *Gene.* 2003;303:11-34.
- 32. Tycko J, Wainberg M, Marinov GK, Ursu O, Hess GT, Ego BK, et al. Mitigation of off-target toxicity in CRISPR-Cas9 screens for essential non-coding elements. *Nat Commun.* 2019:10(1):4063.
- 33. Fulco CP, Nasser J, Jones TR, Munson G, Bergman DT, Subramanian V, et al. Activity-by-contact model of enhancer-promoter regulation from thousands of CRISPR perturbations. *Nat Genet.* 2019;51(12):1664-9.
- 34. Herranz D, Ambesi-Impiombato A, Palomero T, Schnell SA, Belver L, Wendorff AA, et al. A NOTCH1-driven MYC enhancer promotes T cell development, transformation and acute lymphoblastic leukemia. *Nat Med.* 2014;20(10):1130-7.

- 35. Yashiro-Ohtani Y, Wang H, Zang C, Arnett KL, Bailis W, Ho Y, et al. Long-range enhancer activity determines Myc sensitivity to Notch inhibitors in T cell leukemia. *Proc Natl Acad Sci U S A.* 2014.
- 36. Isoda T, Moore AJ, He Z, Chandra V, Aida M, Denholtz M, et al. Non-coding Transcription Instructs Chromatin Folding and Compartmentalization to Dictate Enhancer-Promoter Communication and T Cell Fate. *Cell.* 2017;171(1):103-19 e18.
- 37. Li L, Zhang JA, Dose M, Kueh HY, Mosadeghi R, Gounari F, et al. A far downstream enhancer for murine Bcl11b controls its T-cell specific expression. *Blood*. 2013;122(6):902-11.
- 38. Nagel S, Kaufmann M, Drexler HG, and MacLeod RA. The cardiac homeobox gene NKX2-5 is deregulated by juxtaposition with BCL11B in pediatric T-ALL cell lines via a novel t(5;14)(q35.1;q32.2). *Cancer Res.* 2003;63(17):5329-34.
- 39. Nagel S, Scherr M, Kel A, Hornischer K, Crawford GE, Kaufmann M, et al. Activation of TLX3 and NKX2-5 in t(5;14)(q35;q32) T-cell acute lymphoblastic leukemia by remote 3'-BCL11B enhancers and coregulation by PU.1 and HMGA1. *Cancer Res.* 2007;67(4):1461-71.
- 40. Polonen P, Di Giacomo D, Seffernick AE, Elsayed A, Kimura S, Benini F, et al. The genomic basis of childhood T-lineage acute lymphoblastic leukaemia. *Nature*. 2024;632(8027):1082-91.
- 41. Almeida A, T'Sas S, Pagliaro L, Fijalkowski I, Sleeckx W, Van Steenberge H, et al. Myb overexpression synergizes with the loss of Pten and is a dependency factor and therapeutic target in T-cell lymphoblastic leukemia. *Hemasphere*. 2024;8(3):e51.
- 42. Xie S, Armendariz D, Zhou P, Duan J, and Hon GC. Global Analysis of Enhancer Targets Reveals Convergent Enhancer-Driven Regulatory Modules. *Cell Rep.* 2019;29(9):2570-8 e5.
- 43. Tatarek J, Cullion K, Ashworth T, Gerstein R, Aster JC, and Kelliher MA. Notch1 inhibition targets the leukemia-initiating cells in a Tal1/Lmo2 mouse model of T-ALL. *Blood*. 2011;118(6):1579-90.
- 44. Chiang MY, Shestova O, Xu L, Aster JC, and Pear WS. Divergent effects of supraphysiologic Notch signals on leukemia stem cells and hematopoietic stem cells. *Blood*. 2013:121(6):905-17.
- 45. Tremblay M, Tremblay CS, Herblot S, Aplan PD, Hebert J, Perreault C, et al. Modeling T-cell acute lymphoblastic leukemia induced by the SCL and LMO1 oncogenes. *Genes Dev.* 2010;24(11):1093-105.
- 46. Tremblay CS, Chiu SK, Saw J, McCalmont H, Litalien V, Boyle J, et al. Small molecule inhibition of Dynamin-dependent endocytosis targets multiple niche signals and impairs leukemia stem cells. *Nat Commun.* 2020;11(1):6211.
- 47. Poort VM, Hagelaar R, van Roosmalen MJ, Trabut L, Buijs-Gladdines J, van Wijk B, et al. Transient Differentiation-State Plasticity Occurs During Acute Lymphoblastic Leukemia Initiation. *Cancer Res.* 2024.
- 48. Kuhn R, Schwenk F, Aguet M, and Rajewsky K. Inducible gene targeting in mice. *Science*. 1995;269(5229):1427-9.
- 49. Schlenner SM, Madan V, Busch K, Tietz A, Laufle C, Costa C, et al. Fate mapping reveals separate origins of T cells and myeloid lineages in the thymus. *Immunity*. 2010;32(3):426-36.
- 50. Oguro H, Ding L, and Morrison SJ. SLAM family markers resolve functionally distinct subpopulations of hematopoietic stem cells and multipotent progenitors. *Cell Stem Cell*. 2013;13(1):102-16.
- 51. Pietras EM, Reynaud D, Kang YA, Carlin D, Calero-Nieto FJ, Leavitt AD, et al. Functionally Distinct Subsets of Lineage-Biased Multipotent Progenitors Control Blood Production in Normal and Regenerative Conditions. *Cell Stem Cell*. 2015;17(1):35-46.

- 52. Cheasley D, Pereira L, Lightowler S, Vincan E, Malaterre J, and Ramsay RG. Myb controls intestinal stem cell genes and self-renewal. *Stem Cells*. 2011;29(12):2042-50.
- 53. Thompson MA, Rosenthal MA, Ellis SL, Friend AJ, Zorbas MI, Whitehead RH, et al. c-Myb down-regulation is associated with human colon cell differentiation, apoptosis, and decreased Bcl-2 expression. *Cancer Res.* 1998;58(22):5168-75.
- 54. Kopecki Z, Luchetti MM, Adams DH, Strudwick X, Mantamadiotis T, Stoppacciaro A, et al. Collagen loss and impaired wound healing is associated with c-Myb deficiency. *J Pathol.* 2007:211(3):351-61.
- 55. Vesela B, Svandova E, Smarda J, and Matalova E. Mybs in mouse hair follicle development. *Tissue Cell.* 2014;46(5):352-5.
- 56. Yamamoto N, Tanigaki K, Han H, Hiai H, and Honjo T. Notch/RBP-J signaling regulates epidermis/hair fate determination of hair follicular stem cells. *Curr Biol.* 2003;13(4):333-8.
- 57. Aster JC, Xu L, Karnell FG, Patriub V, Pui JC, and Pear WS. Essential roles for ankyrin repeat and transactivation domains in induction of T-cell leukemia by Notch1. *Mol Cell Biol*. 2000;20(20):7505-15.
- 58. Pear WS, Aster JC, Scott ML, Hasserjian RP, Soffer B, Sklar J, et al. Exclusive development of T cell neoplasms in mice transplanted with bone marrow expressing activated Notch alleles. *J Exp Med.* 1996;183(5):2283-91.
- 59. Weng AP, Nam Y, Wolfe MS, Pear WS, Griffin JD, Blacklow SC, et al. Growth suppression of pre-T acute lymphoblastic leukemia cells by inhibition of notch signaling. *Mol Cell Biol.* 2003;23(2):655-64.
- 60. Schroeter EH, Kisslinger JA, and Kopan R. Notch-1 signalling requires ligand-induced proteolytic release of intracellular domain. *Nature*. 1998;393(6683):382-6.
- 61. Smith S, Tripathi R, Goodings C, Cleveland S, Mathias E, Hardaway JA, et al. LIM domain only-2 (LMO2) induces T-cell leukemia by two distinct pathways. *PLoS One.* 2014;9(1):e85883.
- 62. Clappier E, Cuccuini W, Kalota A, Crinquette A, Cayuela JM, Dik WA, et al. The C-MYB locus is involved in chromosomal translocation and genomic duplications in human T-cell acute leukemia (T-ALL), the translocation defining a new T-ALL subtype in very young children. *Blood.* 2007;110(4):1251-61.
- 63. O'Neil J, Tchinda J, Gutierrez A, Moreau L, Maser RS, Wong KK, et al. Alu elements mediate MYB gene tandem duplication in human T-ALL. *J Exp Med.* 2007;204(13):3059-66
- 64. Lahortiga I, De Keersmaecker K, Van Vlierberghe P, Graux C, Cauwelier B, Lambert F, et al. Duplication of the MYB oncogene in T cell acute lymphoblastic leukemia. *Nat Genet*. 2007;39(5):593-5.
- 65. Liu Y, Easton J, Shao Y, Maciaszek J, Wang Z, Wilkinson MR, et al. The genomic landscape of pediatric and young adult T-lineage acute lymphoblastic leukemia. *Nat Genet*. 2017;49(8):1211-8.
- 66. Mullighan CG, Goorha S, Radtke I, Miller CB, Coustan-Smith E, Dalton JD, et al. Genome-wide analysis of genetic alterations in acute lymphoblastic leukaemia. *Nature*. 2007;446(7137):758-64.
- 67. Mansour MR, Abraham BJ, Anders L, Berezovskaya A, Gutierrez A, Durbin AD, et al. Oncogene regulation. An oncogenic super-enhancer formed through somatic mutation of a noncoding intergenic element. *Science*. 2014:346(6215):1373-7.
- 68. Sanda T, Lawton LN, Barrasa MI, Fan ZP, Kohlhammer H, Gutierrez A, et al. Core transcriptional regulatory circuit controlled by the TAL1 complex in human T cell acute lymphoblastic leukemia. *Cancer Cell.* 2012;22(2):209-21.
- 69. Ramsay RG, and Gonda TJ. MYB function in normal and cancer cells. *Nat Rev Cancer*. 2008;8(7):523-34.

- 70. Kimura S, Polonen P, Montefiori L, Park CS, Iacobucci I, Yeoh AE, et al. Biologic and clinical features of childhood gamma delta T-ALL: identification of STAG2/LMO2 gammadelta T-ALL as an extremely high risk leukemia in the very young. *medRxiv*. 2023.
- 71. Cauwelier B, Dastugue N, Cools J, Poppe B, Herens C, De Paepe A, et al. Molecular cytogenetic study of 126 unselected T-ALL cases reveals high incidence of TCRbeta locus rearrangements and putative new T-cell oncogenes. *Leukemia*. 2006;20(7):1238-44.
- 72. Mansour MR, Sanda T, Lawton LN, Li X, Kreslavsky T, Novina CD, et al. The TAL1 complex targets the FBXW7 tumor suppressor by activating miR-223 in human T cell acute lymphoblastic leukemia. *J Exp Med.* 2013;210(8):1545-57.
- 73. Smith C, Goyal A, Weichenhan D, Allemand E, Mayakonda A, Toprak U, et al. TAL1 activation in T-cell acute lymphoblastic leukemia: a novel oncogenic 3' neo-enhancer. *Haematologica*. 2023;108(5):1259-71.
- 74. Aplan PD, Lombardi DP, Ginsberg AM, Cossman J, Bertness VL, and Kirsch IR. Disruption of the human SCL locus by "illegitimate" V-(D)-J recombinase activity. *Science*. 1990;250(4986):1426-9.
- 75. Levy S, Hannenhalli S, and Workman C. Enrichment of regulatory signals in conserved non-coding genomic sequence. *Bioinformatics*. 2001;17(10):871-7.
- 76. Calvello R, Cianciulli A, Mitolo V, Porro A, and Panaro MA. Conservation of Intronic Sequences in Vertebrate Mitochondrial Solute Carrier Genes (Zebrafish, Chicken, Mouse and Human). *Noncoding RNA*. 2019;5(1).
- 77. Cianciulli A, Calvello R, and Panaro MA. Determinism and randomness in the evolution of introns and sine inserts in mouse and human mitochondrial solute carrier and cytokine receptor genes. *Comput Biol Chem.* 2015;55:49-59.
- 78. Unnikrishnan A, Guan YF, Huang Y, Beck D, Thoms JA, Peirs S, et al. A quantitative proteomics approach identifies ETV6 and IKZF1 as new regulators of an ERG-driven transcriptional network. *Nucleic Acids Res.* 2016;44(22):10644-61.
- 79. Klein JC, Agarwal V, Inoue F, Keith A, Martin B, Kircher M, et al. A systematic evaluation of the design and context dependencies of massively parallel reporter assays. *Nat Methods*. 2020:17(11):1083-91.
- 80. Xue JR, Mackay-Smith A, Mouri K, Garcia MF, Dong MX, Akers JF, et al. The functional and evolutionary impacts of human-specific deletions in conserved elements. *Science*. 2023;380(6643):eabn2253.
- 81. Feng Y, Xie N, Inoue F, Fan S, Saskin J, Zhang C, et al. Integrative functional genomic analyses identify genetic variants influencing skin pigmentation in Africans. *Nat Genet*. 2024;56(2):258-72.
- 82. Agarwal V, Inoue F, Schubach M, Penzar D, Martin BK, Dash PM, et al. Massively parallel characterization of transcriptional regulatory elements. *Nature*. 2025;639(8054):411-20.
- 83. Consortium I. Deciphering the impact of genomic variation on function. *Nature*. 2024;633(8028):47-57.
- 84. Petrovic J, Zhou Y, Fasolino M, Goldman N, Schwartz GW, Mumbach MR, et al. Oncogenic Notch Promotes Long-Range Regulatory Interactions within Hyperconnected 3D Cliques. *Mol Cell*. 2019:73(6):1174-90 e12.
- 85. Trimarchi T, Bilal E, Ntziachristos P, Fabbri G, Dalla-Favera R, Tsirigos A, et al. Genome-wide mapping and characterization of Notch-regulated long noncoding RNAs in acute leukemia. *Cell.* 2014;158(3):593-606.
- 86. Gu TL, Goetz TL, Graves BJ, and Speck NA. Auto-inhibition and partner proteins, corebinding factor beta (CBFbeta) and Ets-1, modulate DNA binding by CBFalpha2 (AML1). *Mol Cell Biol.* 2000;20(1):91-103.

- 87. Farnaby W, Koegl M, Roy MJ, Whitworth C, Diers E, Trainor N, et al. BAF complex vulnerabilities in cancer demonstrated via structure-based PROTAC design. *Nat Chem Biol.* 2019;15(7):672-80.
- 88. Xiao L, Parolia A, Qiao Y, Bawa P, Eyunni S, Mannan R, et al. Targeting SWI/SNF ATPases in enhancer-addicted prostate cancer. *Nature*. 2022;601(7893):434-9.
- 89. Aoki K, Hyuga M, Tarumoto Y, Nishibuchi G, Ueda A, Ochi Y, et al. Canonical BAF complex regulates the oncogenic program in human T-cell acute lymphoblastic leukemia. *Blood.* 2024;143(7):604-18.
- 90. Rahman S, Magnussen M, León T, Farah N, Abraham B, Li Z, et al. Activation of the LMO2 Oncogene in T-ALL through a Somatically Acquired Neomorphic Promoter *ASH Annual Meeting Abstracts*. 2016;128(22).
- 91. Tan SH, Leong WZ, Ngoc PCT, Tan TK, Bertulfo FC, Lim MC, et al. The enhancer RNA ARIEL activates the oncogenic transcriptional program in T-cell acute lymphoblastic leukemia. *Blood.* 2019.
- 92. Ong JZL, Tan TK, Wang L, Tan SH, and Sanda T. Regulatory mechanisms and context-dependent roles of TAL1 in T-cell acute lymphoblastic leukemia. *Haematologica*. 2023.
- 93. Noronha EP, Marques LVC, Andrade FG, Thuler LCS, Terra-Granado E, Pombo-de-Oliveira MS, et al. The Profile of Immunophenotype and Genotype Aberrations in Subsets of Pediatric T-Cell Acute Lymphoblastic Leukemia. *Front Oncol.* 2019;9:316.
- 94. Lieu YK, Kumar A, Pajerowski AG, Rogers TJ, and Reddy EP. Requirement of c-myb in T cell development and in mature T cell function. *Proc Natl Acad Sci U S A*. 2004;101(41):14853-8.
- 95. Lee PP, Fitzpatrick DR, Beard C, Jessup HK, Lehar S, Makar KW, et al. A critical role for Dnmt1 and DNA methylation in T cell development, function, and survival. *Immunity*. 2001;15(5):763-74.
- 96. Tottone L, Lancho O, Loh JW, Singh A, Kimura S, Roels J, et al. A Tumor Suppressor Enhancer of PTEN in T-cell development and leukemia. *Blood Cancer Discov*. 2021;2(1):92-109.
- 97. Tan SH, Tan TK, Yokomori R, Liao M, Huang XZ, Yeoh AEJ, et al. TAL1 hijacks MYCN enhancer that induces MYCN expression and dependence on mevalonate pathway in T-cell acute lymphoblastic leukemia. *Leukemia*. 2023;37(10):1969-81.
- 98. Lieu YK, and Reddy EP. Conditional c-myb knockout in adult hematopoietic stem cells leads to loss of self-renewal due to impaired proliferation and accelerated differentiation. *Proc Natl Acad Sci U S A.* 2009;106(51):21689-94.
- 99. Clarke ML, Lemma RB, Walton DS, Volpe G, Noyvert B, Gabrielsen OS, et al. MYB insufficiency disrupts proteostasis in hematopoietic stem cells, leading to age-related neoplasia. *Blood.* 2023;141(15):1858-70.
- 100. Mucenski ML, McLain K, Kier AB, Swerdlow SH, Schreiner CM, Miller TA, et al. A functional c-myb gene is required for normal murine fetal hepatic hematopoiesis. *Cell*. 1991;65(4):677-89.
- 101. Kim H, Tan TK, Lee DZY, Huang XZ, Ong JZL, Kelliher MA, et al. Oncogenic dependency on SWI/SNF chromatin remodeling factors in T-cell acute lymphoblastic leukemia. *Leukemia*. 2024.
- 102. Dreier MR, Walia J, and de la Serna IL. Targeting SWI/SNF Complexes in Cancer: Pharmacological Approaches and Implications. *Epigenomes*. 2024;8(1).
- 103. Economides AN, Frendewey D, Yang P, Dominguez MG, Dore AT, Lobov IB, et al. Conditionals by inversion provide a universal method for the generation of conditional alleles. *Proc Natl Acad Sci U S A.* 2013;110(34):E3179-88.
- 104. Kodgule R, Goldman JW, Monovich AC, Saari T, Aguilar AR, Hall CN, et al. ETV6 Deficiency Unlocks ERG-Dependent Microsatellite Enhancers to Drive Aberrant Gene Activation in B-Lymphoblastic Leukemia. *Blood Cancer Discov.* 2023;4(1):34-53.

- 105. Roels J, Kuchmiy A, De Decker M, Strubbe S, Lavaert M, Liang KL, et al. Distinct and temporary-restricted epigenetic mechanisms regulate human alphabeta and gammadelta T cell development. *Nat Immunol.* 2020;21(10):1280-92.
- 106. Kong AT, Leprevost FV, Avtonomov DM, Mellacheruvu D, and Nesvizhskii AI. MSFragger: ultrafast and comprehensive peptide identification in mass spectrometry-based proteomics. *Nat Methods*. 2017;14(5):513-20.
- 107. da Veiga Leprevost F, Haynes SE, Avtonomov DM, Chang HY, Shanmugam AK, Mellacheruvu D, et al. Philosopher: a versatile toolkit for shotgun proteomics data analysis. *Nat Methods*. 2020;17(9):869-70.
- 108. Djomehri SI, Gonzalez ME, da Veiga Leprevost F, Tekula SR, Chang HY, White MJ, et al. Quantitative proteomic landscape of metaplastic breast carcinoma pathological subtypes and their relationship to triple-negative tumors. *Nat Commun.* 2020;11(1):1723.

#### Figure legends

Figure 1. The hematopoietic stem cell MYB enhancer (H-Me) is a top-ranked essential regulatory element in T-ALL cells that appears relatively quiescent in the developmental stages from which T-ALL initiates. A) Schematic of the CRISPRi screen to identify essential ETS1-dependent enhancers in the THP-6 T-ALL cell line. B) CRISPRi essentiality screen results. MAGeCK analysis in Table S2. C) ATAC-seq profiles of the murine H-Me in long-term HSCs (LT-HSCs) through T-cell development (Immgen). D) ATAC-seq profiles of the human H-Me in sorted thymocytes subsets (GSE151075 (105)). D1 = Donor 1; D2 = Donor; HSC=CD34<sup>+</sup> cord blood; ETP/DN2 = CD34<sup>+</sup>CD4<sup>-</sup>CD1<sup>-</sup>; DN3/DN4 = CD34<sup>+</sup>CD4<sup>-</sup>CD1<sup>+</sup>; ISP = CD28<sup>+</sup>CD4<sup>+</sup>CD3<sup>-</sup>CD8<sup>-</sup>; DP = CD4<sup>+</sup>CD8<sup>+</sup>; SP = single positive. E) H3K27ac ChIP-seq profiles of normal thymocyte subsets at the H-Me and the N-Me in 50kb windows (St. Jude Cloud at https://viz.stjude.cloud/mullighan-lab/collection/the-genomic-basis-of-childhood-t-lineageacute-lymphoblastic-leukemia~29). F) Histone chromatin profiles of DP cells of 4 donors (D1-D4; BLUEPRINT project) comparing a silenced region to the *MYB-AHI1* region.

Figure 2. The H-Me normally restricts hematopoietic stem cell (HSC) numbers and maintains early T-cell precursors (ETPs) under steady state conditions. A) Schematic of the floxed H-Me allele (f). SA=Rabbit beta-globin splice acceptor sequence (103). B) qRT-PCR of *Myb* and *Ahi1* in sorted LT-HSCs (CD150<sup>+</sup>CD48<sup>-</sup>Lineage Sca-1<sup>+</sup>Kit<sup>+</sup> (LSK)) cells from *Mx1Cre H-Me*<sup>Δ/Δ</sup> (Δ/Δ) and littermate control *Mx1Cre* (+/+) mice. C-G) Representative bone marrow Lineage flow cytometry plots (C) and absolute numbers of LT-HSCs (D), LSK (E), MPP/ST-HSC (F, CD150<sup>+</sup>CD48<sup>-</sup> LSKs), and LMPPs (G, Lineage Sca-1<sup>+</sup>Kit<sup>hi</sup>Flt3<sup>hi</sup>). H-M) Representative thymus Lineage flow cytometry plots (H) and absolute numbers of ETP (I, Lineage CD44<sup>+</sup>CD25<sup>-</sup>cKit<sup>hi</sup>), DN2a (J, Lineage CD44<sup>+</sup>CD25<sup>+</sup>cKit<sup>hi</sup>), DN2b (K, Lineage CD44<sup>+</sup>CD25<sup>+</sup>cKit<sup>ho</sup>), DN3 (L, Lineage CD44<sup>+</sup>CD25<sup>+</sup>), and DN4 (M, Lineage CD44<sup>-</sup>CD25<sup>-</sup>) cells. N) *Myb* qRT-PCR in sorted DN cells from

 $II7rCre\ H-Me^{A/\Delta}\ (\Delta/\Delta)$  and littermate control  $II7rCre\ (+/+)$  mice. Unpaired 2-tailed t-test. \*P<0.05; \*\*P<0.01; \*\*\*P<0.001.

Figure 3. The H-Me is important for long-term HSC self-renewal under stress conditions.

A) Schematic of serial competitive BMT experiment. B-I) Peripheral blood analysis of indicated subsets tracking %donor (CD45.2<sup>+</sup>)-derived cells after the first BMT (B-E) and the second BMT (F-I). J-L) Representative Lineage<sup>-</sup> flow cytometry plots (J) and %donor-derived (CD45.2<sup>+</sup>) analysis of LT-HSCs (K) and MPP/ST-HSCs (L) at 16 weeks after the second BMT. Unpaired 2-tailed t-test. \*P<0.05; \*\*P<0.01; \*\*\*P<0.001; \*\*\*\*P<0.0001.

Figure 4. The H-Me limits myeloid expansion and HSC loss with aging. A-J) WBC (A, F), neutrophil counts (B, G), monocyte counts (C, H), hemoglobin concentrations (D, I), and platelet counts (E, J) comparing 8-month-old (A-E) and 12-month-old (F-J) indicated mice. K-O) Representative flow cytometric plots (K) and absolute numbers of LT-HSCs (L), MPP/ST-HSCs (M), hematopoietic stem and progenitor cells (LSK, N), and total BM cells (O) in 1-year old mice as defined in Fig. 2. P-V) Representative flow cytometric plots (P) and absolute numbers of ETP (Q), DN2a (R), DN2b (S), DN3 (T), DN4 (U), and total thymocyte cells (V) as defined in Fig. 1. Unpaired 2-tailed t-test. \*P<0.05; \*\*P<0.01; \*\*\*P<0.001.

**Figure 5.** The H-Me is an essential regulatory element for T-ALL leukemogenesis in multiple genetically engineered mouse models. A) Schematic showing generation of Notch-induced T-ALL by transducing ΔΕ/Notch1 retrovirus (59, 60) into hematopoietic stem and progenitor cells from H-Me<sup>-/-</sup> mice or littermate controls followed by transplantation. B-D) Representative flow cytometry plots (B), GFP<sup>+</sup> blast counts at 4 weeks after transplant (C), and leukemia-free survival curves (D) for the experiment in (A). E) Schematic showing generation of Notch-induced T-ALL

by transducing  $\Delta E/Notch1$  retrovirus into hematopoietic stem and progenitor cells from Mx1Cre  $H-Me^{t/f}$  mice and Mx1Cre littermate controls followed by transplantation and injection of pl-pC to delete the H-Me. F-H) Representative flow cytometry plots (F), GFP<sup>+</sup> blast counts at 4 weeks after injection of pl-pC (G), and leukemia-free survival curves (H) for the experiment in (E). I-J) Lmo2-tg  $H-Me^{-t/-}$  and littermate control  $H-Me^{-t/+}$  mice were observed for survival (I) and development of T-ALL, which was confirmed by flow cytometry of thymic mass (#33, #98, and #61) or spleen mass (#772) (J). Unpaired 2-tailed t-test and log-rank test. \*\*\*\*P<0.0001.

Figure 6. The H-Me is co-amplified with *MYB* in nearly all human T-ALL patients with *MYB* amplifications. A) Amplified region in primary human T-ALL in the WGS dataset from AALL0434 (N=1,309 patients) (40). Each row is a unique patient (N=115). Bar shows the *MYB*-to-H-Me region. B-C) WGS tracks showing sequence reads in the *MYB-AHI1* region including the H-Me in THP-6 cells (B) and other T-ALL cell lines used in this study (C).

Figure 7. The H-Me is important in diverse models of human T-ALL maintenance. A) ATAC-seq profiles (green) of a panel of T-ALL cell lines and primary samples across the *MYB* TAD. ETS1 and H3K27ac tracks in THP-6 cells are shown in blue (GSE138516). MYB enhancers "A" and "B" were previously described (67-69). ATAC-seq datasets from GSE129086, GSE110630, GSE263585, GSE263977, and GSE225559. TAD datasets from GSE134761. B-G) THP-6 (B, E), Jurkat (C, F), and MOLT14 (D, G) cells were transduced with constitutive (THP-6) or dox-inducible (Jurkat, MOLT14) dCas9-KRAB and sgRNAs against the H-Me or the *MYB* promoter and then tested for expression of *MYB* (B-D) and measured for cell growth (E-G). *HBS1L* and *AHI1* are flanking genes of *MYB*. H-J) CEM cells, related to THP-6, transduced with indicated sgRNAs were injected into NSG mice and 2-5 days later treated with doxycycline in drinking water to activate dCas9-KRAB-GFP. Representative GFP/hCD45.2 flow cytometry plots of peripheral blood at 4 weeks after injection (H), GFP\*/hCD45\* blast counts (I) and survival (log-rank test P values, J)

were measured. N=9 (control); N=10 (PE); N=10 (H-Me). NT=non-targeting; PE=pan-essential gene *RPL34*. 1-way ANOVA test. \*P<0.05; \*\*P<0.01; \*\*\*P<0.001; \*\*\*\*P<0.0001.

Figure 8. ETS1 recruits cBAF through the ETS motif in the H-Me to activate MYB expression in THP-6/CEM cells. A-B) Western blot of ETS1 and MYB proteins (A) and MYB gRT-PCR (B) showing the effect of 500nM dTAG<sup>V</sup>-1 in degrading ETS1 in ETS1-FKBP<sup>F36V</sup> knock-in THP-6 cells. C-D) Representative Western blots (C) and quantitative Image J analyses (D) showing effect of the ETS motif mutation on ETS1 binding (p54 and p42 isoforms) in "reverse ChIP" in THP-6 cells. E) Normalized abundance plot of transcriptional regulators that were pulled down by "reverse ChIP" and identified by mass spectrometry comparing wildtype and ETS motif mutated H-Me; and analyzed with PD (Thermo Fisher Proteome Discoverer) and FragPipe (106-108). Full results are in Table S3. F-H) Sequences of homozygous partially mutated ETS sites in the 3 H-Me alleles (F), ETS1 qChIP at the H-Me (G); and MYB qRT-PCR (H) in a subclone of ETS1-FKBP<sup>F36V</sup> knockin THP-6 cells after CRISPR/Cas9 editing and homology directed repair (HDR). I) Venn diagram showing intersection of the H-Me and ETS1 interactomes ranked by strength of interaction with Flag-ETS1. The H-Me interactome was supplemented with transcriptional regulators that met Padj<0.1/LFC>0 criteria by Proteome Discoverer. Full results are in Table S4 and S5. J) Flag co-IP assay in vector-transduced (Ctrl) and Flag-ETS1-transduced CEM cells showing interactions with endogenous SMARCC1 and SMARCB1. K) Reciprocal co-IP assay comparing IgG and anti-SMARCC1 pulldowns in CEM cells to detect interactions with endogenous ETS1. L) ARID1A and PBRM1 qChIP using primers at the H-Me peak center or a negative control site 1.25kb downstream in ETS1-FKBPF36V knock-in THP-6 cells treated with 500nM dTAGV-1 (dTAG) to degrade ETS1. M) ATAC-seq profiles of the MYB topologically associating domain (TAD) in ETS1-FKBP<sup>F36V</sup> knock-in THP-6 cells treated with dTAG to degrade ETS1. DeSeq2 analysis. N) MYB qRT-PCR in ETS1-FKBP<sup>F36V</sup> knock-in THP-6 cells with mutated ETS-binding sites in the H-Me (F) treated with DMSO vs AU-15330. O) Western blot for indicated proteins in DMSO-treated or AU-15330-treated T-ALL cells. 1-way ANOVA test. \*P<0.05; \*\*P<0.01; \*\*\*\*P<0.001; \*\*\*\*P<0.0001.

